

## STEAM REFORMING OF ETHANOL ON FERRITES

L. Y. Dolgikh, I. L. Stolyarchuk, L. A. Staraya,  
and Y. I. Pyatnitsky

UDC 544.47:544.344

*The results of the authors' investigations of steam reforming of ethanol (SRE) on nanosized ferrites with spinel structure  $MFe_2O_4$  ( $M = Mg, Mn, Fe, Co, Ni, Cu, Zn$ ) are summarized. The highest yields of the target product hydrogen were obtained on Mg, Mn, and Fe ferrites. A close to stoichiometric yield of  $H_2$  was obtained on nanosized  $MnFe_2O_4$ . A probable scheme for the mechanism of SRE, containing redox and acid–base stages, is proposed.*

**Key words:** ethanol, steam reforming, oxide catalysts, hydrogen.

Steam reforming of ethanol is a prospective method for the production of hydrogen from renewable feedstock for subsequent use as a motor fuel or in fuel cells. In the full conversion of ethanol in the SRE process by the reaction



the hydrogen is formed both from the ethanol (50 mole %) and from water (50 mole %), which makes the process particularly attractive. It is also important that if bioethanol obtained from plant feedstock is used carbon dioxide does not accumulate in the atmosphere since the release of  $CO_2$  into the atmosphere in reaction (I) is fully compensated by its consumption during growth of the plants.

According to the reviews [1–5] a large number of papers have been devoted to investigation of the steam reforming of ethanol, and in most of them supported metallic catalysts were used for SRE. Only a limited number of other types of catalysts have been studied in this reaction, and they include simple and complex oxides. The catalytic properties of  $MgO$ ,  $Al_2O_3$ ,  $ZnO$ ,  $V_2O_5$ ,  $La_2O_3$ ,  $CeO_2$ , and  $Sm_2O_3$  were investigated in [6]. Most of the investigated simple oxides were active in the conversion of ethanol. Here products from steam reforming of ethanol were observed at the oxides  $V_2O_5$ ,  $La_2O_3$ ,  $CeO_2$ , and  $Sm_2O_3$  (the oxides of metals with variable valence), which have oxidation–reduction characteristics. Most effective was the oxide  $ZnO$ , which has redox characteristics. Complex oxides with a spinel structure  $MAI_2O_4$  ( $M = Cu, Zn, or Ni$ ) were highly effective in SRE [7]. The catalytic characteristics of complex oxides  $NiM_2O_4$  ( $M = Al, Mn, Fe$ ) were investigated in [8]. Spinel  $NiAl_2O_4$  exhibited high activity and selectivity at 823 K; the crystal structure of  $NiAl_2O_4$  remained practically unchanged under the reaction conditions, whereas the spinels  $NiMn_2O_4$  and  $NiFe_2O_4$  decomposed to some degree or other [8]. Catalysts based on the perovskites  $La_2NiO_4$ ,  $LaFe_yNi_{1-y}O_3$ , and  $LaCo_{1-x}Zn_xO_3$  also proved fairly active and selective although they decomposed in the course of catalysis [9, 10]. High activity in SRE was exhibited by a catalyst based on cobalt hydrotalcite [11]; it is notable that only traces of metallic cobalt were identified after the reaction, i.e., cobalt in the oxidized state is the active particle in the

---

L. V. Pysarzhevsky Institute of Physical Chemistry, National Academy of Sciences of Ukraine, Nauky Ave., 31, Kyiv 03028, Ukraine. E-mail: [ldolgykh@inphyschem-nas.kiev.ua](mailto:ldolgykh@inphyschem-nas.kiev.ua). Translated from *Teoreticheskaya i Éksperimental'naya Khimiya*, Vol. 54, No. 5, pp. 318–325, September–October, 2018. Original article submitted June 16, 2018; revision submitted June 25, 2018.

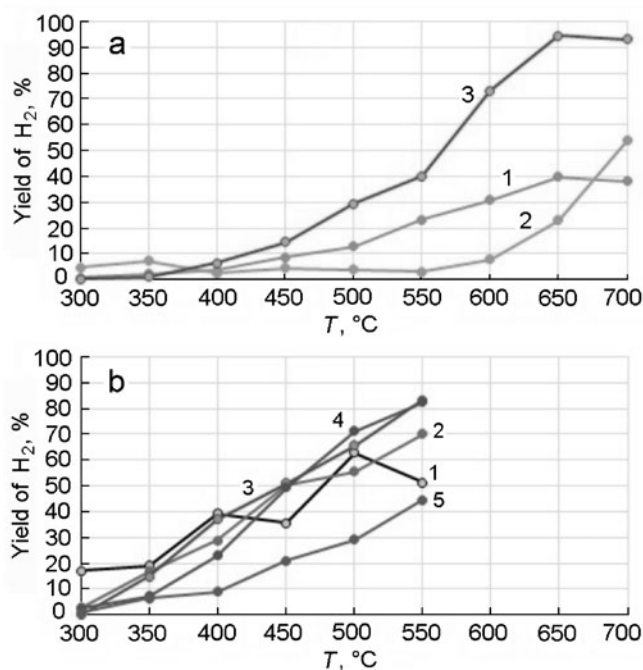


Fig. 1. Temperature dependence of yield of hydrogen at nanocatalysts NiFe<sub>2</sub>O<sub>4</sub> (1), CoFe<sub>2</sub>O<sub>4</sub> (2), and MnFe<sub>2</sub>O<sub>4</sub> (3) obtained by thermal decomposition of the heteronuclear complexes (a) and at the catalysts CuFe<sub>2</sub>O<sub>4</sub> (1), FeFe<sub>2</sub>O<sub>4</sub> (2), MnFe<sub>2</sub>O<sub>4</sub> (3), MgFe<sub>2</sub>O<sub>4</sub> (4), and ZnFe<sub>2</sub>O<sub>4</sub> (5) obtained by the coprecipitation method (b).

mixed oxide catalyst. The Fe<sub>x</sub>Co<sub>3-x</sub>O<sub>4</sub> catalysts, for which metal phases were not detected after catalysis with  $x > 0.15$ , were highly effective in SRE [12].

In the present work we present the results of our investigations of the steam reforming of ethanol on complex oxide catalysts: ferrites MFe<sub>2</sub>O<sub>4</sub> (M = Mg, Mn, Fe, Co, Ni, Cu, Zn) [13-21]. Samples of Mn, Co, and Ni ferrites were prepared by thermal decomposition of [MFe<sub>2</sub>O(CH<sub>3</sub>COO)<sub>6</sub>(H<sub>2</sub>O)<sub>3</sub>]·2H<sub>2</sub>O (M = Mn, Co, Ni) by the method described in [22]. According to TEM and XRD the initial samples consisted of nanoparticles of the respective ferrites with an average diameter of about 8 nm and a narrow particle size distribution [15]. Manganese ferrite was also prepared by coprecipitation, as also were the ferrites of Fe, Mg, and Zn [15, 21]. Electron diffraction data for the samples prepared in this way showed the presence of crystalline phases in the corresponding ferrites with spinel structures.

The catalytic properties of the ferrites in the SRE process were investigated in a flow-type quartz reactor with molar ratio H<sub>2</sub>O/C<sub>2</sub>H<sub>5</sub>OH = 19 (2.7 mole % C<sub>2</sub>H<sub>5</sub>OH, 50 mole % H<sub>2</sub>O, remainder N<sub>2</sub>), which is close to the water/ethanol ratio in bioethanol produced by the fermentation of biomass, and the reaction mixture flow rate was 0.17 mol/h. All the obtained ferrites exhibited catalytic activity in SRE. Figure 1a and b shows the temperature dependence of the yield of hydrogen for the ferrite catalysts. The yield of hydrogen was taken as 100% if six moles of hydrogen were formed for one mole of ethanol added to the reactor in accordance with the stoichiometry of reaction (I).

The composition of the Mg, Mn, Fe, and Zn ferrites did not change in the course of catalysis [13, 20, 21] (only sintering of the nanoparticles occurred), while the Co, Ni, and Cu ferrites were partly or completely reduced to the respective metals by the action of the reaction mixture [15, 18, 21].

The highest yield of hydrogen (94.6%) was obtained for the nanosized MnFe<sub>2</sub>O<sub>4</sub> obtained by decomposition of the heteronuclear complex at 650 °C (Fig. 1a). The second highest yield of hydrogen (84.3%) was obtained at 550 °C with MnFe<sub>2</sub>O<sub>4</sub> obtained by coprecipitation (Fig. 1b). It is not impossible that a higher yield could be obtained with this catalyst if the

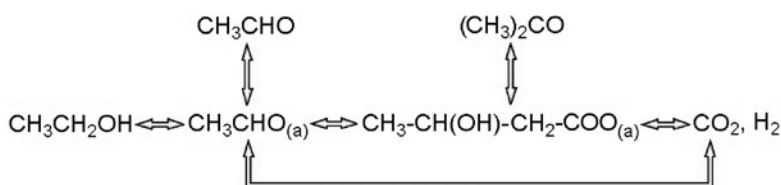
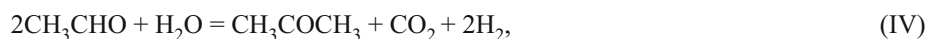
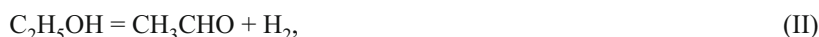


Fig. 2. Scheme of the conversion of ethanol at ferrites.

catalysis temperature was increased since, as seen from Fig. 1b, the yield of hydrogen has a tendency to increase with increase of temperature.

The main side products observed during SRE on ferrites were acetaldehyde, acetone, and carbon oxides. Exceptions were the nickel and cobalt ferrites, where the formation of acetone was not observed during catalysis. The yield of hydrogen was reduced by the formation of side products. From our data and from the published data [1, 3, 23, 24] it is possible to propose the following scheme for the conversion of ethanol in the SRE process on ferrites (Fig. 2, the subscript “a” signifies the adsorbed state).

The scheme includes the target reaction (I) and reactions leading to the formation of the main side products:



At higher temperatures the formation of CO was also observed at  $\text{NiFe}_2\text{O}_4$  (550-700 °C),  $\text{CoFe}_2\text{O}_4$  (600-700 °C), and  $\text{MnFe}_2\text{O}_4$  (700 °C); the formation of CO was not observed on the other ferrites. The side products include  $\text{C}_1$ - $\text{C}_3$  hydrocarbons, which in most cases were formed in relatively small amounts.

The mechanism of the SRE process as a whole includes mechanisms of two types: oxidation–reduction and acid–base [19-21]. The oxidation–reduction mechanism is confirmed convincingly by the data obtained for  $\text{FeFe}_2\text{O}_4$  and  $\text{NiFe}_2\text{O}_4$  ferrites in [25, 26]. In these papers the SRE process was conducted by delivering the ethanol vapor and steam alternately to the ferrite catalyst at 450 °C. The delivery times of the reagents to the catalyst varied from 1 h to 2 min. In the long reduction stage of the cycle (1 h) the conversion of ethanol was close to 100%, and the products were  $\text{CO}_2$  and  $\text{H}_2$  and also CO,  $\text{H}_2\text{O}$ ,  $\text{CH}_4$ , carbon, and acetone (observed in the first 10-15 min). The ferrites were reduced in the ethanol atmosphere with the formation of metallic iron and nickel. In the following oxidation stage the structure of the ferrites was restored under the influence of the steam. Apart from hydrogen CO and  $\text{CO}_2$  were also formed at this stage as a result of interaction between the water molecules and the surface carbon. Cyclic delivery of ethanol vapor and steam with short reaction times (the reactions were conducted with  $\text{FeFe}_2\text{O}_4$  [26]) did not lead to change in the structure of the ferrite. Such behavior provides an important argument in favor of the oxidation–reduction mechanism for the SRE process at ferrites under stationary conditions.

At the same time, the individual reactions of the SRE process can include an acid–base stage. Such a reaction may include dehydrogenation of the ethanol to acetaldehyde (II). A scheme for the probable heterolytic mechanism of the reaction on ferrites is presented in Fig. 3. The main features of this mechanism were taken from [27-29], in which a mechanism involving the dehydrogenation of propane to propylene at single  $\text{M}^{\text{II}}$  centers ( $\text{M} = \text{Zn}, \text{Co}, \text{Fe}$ ) in a matrix of  $\text{SiO}_2$  was established.

The surface cations of the metals in the ferrites exhibit the characteristics of Lewis acid centers with oxygen anions as basic centers. Interaction of the ethanol with the acid–base pair of the centers leads to heterolytic cleavage of the O–H bond in the ethanol with the formation of an ethoxy intermediate localized at the metal ion (the Lewis acid center) and a proton localized on a surface oxygen ion (the basic center).

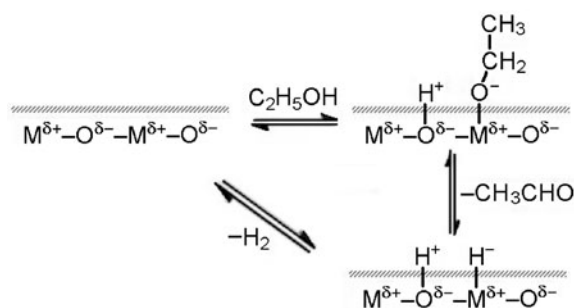
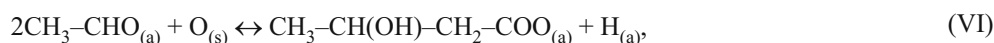


Fig. 3. Scheme of the probable mechanism of dehydrogenation of ethanol to acetaldehyde on the ferrites.

At the next stage  $\beta$ -elimination of a  $H^-$  ion from a C–H bond of the ethoxy particle occurs, and the  $H^-$  combines with a surface metal ion with desorption of an acetaldehyde molecule. The catalytic cycle closes with recombination of the hydride ion and proton to form a molecule of hydrogen in the gas phase.

In our opinion such a mechanism is to be expected for the Mg, Mn, Fe, and Zn ferrites, the chemical composition of which did not change under the action of the reaction mixture in the SRE process. It seems less likely for the  $CuFe_2O_4$  ferrite. This ferrite proved much more active and selective with respect to acetaldehyde than the other investigated ferrites [18, 21]. With this ferrite at an initial temperature of 300 °C in the catalytic experiments the yield of acetaldehyde amounted to 90%, which is not much lower than the thermodynamically possible yield. The high activity of  $CuFe_2O_4$  may be due to the readily occurring reversible  $Cu^{2+} \leftrightarrow Cu^+$  transition on the surface of the copper ferrite, and a homolytic (redox) mechanism of transformation of ethanol into acetaldehyde is thus realized. In any case the copper ferrite can be included among prospective catalysts for the important dehydrogenation of ethanol to acetaldehyde.

The desorption of acetaldehyde most likely includes intermediate formation of an adsorbed particle of  $CH_3CHO_{(a)}$ , which initiates the subsequent reaction paths of the SRE process and particularly transformation into acetone by the aldol condensation mechanism as in the following mechanism for oxide catalysts proposed in [30] and confirmed in [31, 32]:



where  $O_{(s)}$  is the surface oxygen in the crystal lattice of the ferrite.

As known, the aldol condensation is catalyzed by acids or bases; in the case of the SRE process on ferrites condensation takes place with participation of the acid or base centers of the catalyst. The overall conversion of acetaldehyde or ethanol into acetone also includes a redox reaction involving surface oxygen. Removal of the surface oxygen in stage (VI) leads to the formation of surface oxygen vacancies. The loss of oxygen is compensated by interaction of the water with the reduced surface centers according to reaction (VIII), as was observed for  $CeO_2$  [31] and for certain other catalysts [32]:



where  $\square_{(s)}$  represents surface oxygen vacancies.

The oxygen vacancy can be represented in greater detail as  $(Fe^{2+}\square Fe^{2+})_{(s)}$ , which is transformed by reaction (VIII) into  $[Fe^{3+}O^{2-}Fe^{3+}]_{(s)}$ . We note also that reaction (VIII) plays an important role in the SRE process since it is possible from it to obtain up to 50 mole % of hydrogen from such a cheap feedstock as water.

Oxygen vacancies appear in the ferrites not only during the formation of acetone but also as a result of reduction of the surface ions of the metals by other gaseous organic compounds or by their fragments ( $CH_{3(a)}$ ,  $CH_{2(a)}$ ,  $CO_{(a)}$ ) and by hydrogen

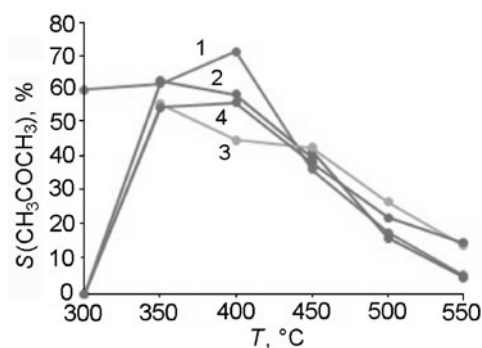
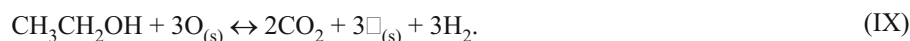


Fig. 4. Temperature dependence of the selectivity to acetone on ferrites  $\text{FeFe}_2\text{O}_4$  (1),  $\text{MnFe}_2\text{O}_4$  (2),  $\text{MgFe}_2\text{O}_4$  (3), and  $\text{ZnFe}_2\text{O}_4$  (4).

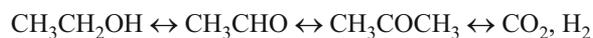
(which is the main reducing agent at elevated temperatures). The overall reduction stage in the SRE process can be represented as follows:



The concentration of oxygen vacancies in the ferrites can vary within certain limits without change in the crystalline phase of the ferrite. However, the crystalline phase is destroyed if it becomes too high, as observed in the ferrites  $\text{NiFe}_2\text{O}_4$ ,  $\text{CoFe}_2\text{O}_4$ , and  $\text{CuFe}_2\text{O}_4$ .

The selectivity toward acetone for the ferrites  $\text{MgFe}_2\text{O}_4$ ,  $\text{MnFe}_2\text{O}_4$ ,  $\text{FeFe}_2\text{O}_4$ , and  $\text{ZnFe}_2\text{O}_4$  that did not undergo reduction during catalysis is presented in Fig. 4.

As seen from Fig. 4, the selectivity to acetone passes through a maximum with increase of temperature. If the overall scheme for the transformation of ethanol is taken into account (Fig. 2), this indicates that the SRE process takes place in consecutive stages:



or, which is particularly characteristic of  $\text{FeFe}_2\text{O}_4$ , according to the reaction path:



(i.e., without the intermediate formation of acetaldehyde in the gas phase).

Maximum selectivity to acetone was observed with  $\text{FeFe}_2\text{O}_4$  at 400 °C (Fig. 4). According to the stoichiometry of reaction (III) the maximum selectivity is 75% to acetone and 25% to  $\text{CO}_2$  since 3/4 of the ethanol molecules are converted into acetone and 1/4 into  $\text{CO}_2$ . As seen from Table 1, the experimental values of the selectivity to acetone and  $\text{CO}_2$  for  $\text{FeFe}_2\text{O}_4$  at 400 °C are close to their theoretical values; according to data in [16, 19] the same was observed for iron oxide  $\text{Fe}_2\text{O}_3$ . (In the course of the SRE process  $\text{Fe}_2\text{O}_3$  is converted into  $\text{FeFe}_2\text{O}_4$ .)

For comparison Table 1 gives the equilibrium values for the conversion of ethanol and the selectivity to the products calculated for the conversion of ethanol into acetaldehyde and acetone with the composition of the initial reaction mixture, 2.7 mole %  $\text{C}_2\text{H}_5\text{OH}$ , 50 mole %  $\text{H}_2\text{O}$ , remainder  $\text{N}_2$ , that was used in the experiments. The results show that the catalytic conversion of ethanol into acetone is close to equilibrium, and further conversion of acetone into  $\text{CO}_2$  and  $\text{H}_2$  is still greatly retarded at 400 °C.

TABLE 1. Experimental and Equilibrium Values for the Conversion of Ethanol and Product Selectivity at 400 °C

| Conversion of ethanol, %         |      | Selectivity, %                    |                 |                     |                |
|----------------------------------|------|-----------------------------------|-----------------|---------------------|----------------|
|                                  |      | CH <sub>3</sub> COCH <sub>3</sub> | CO <sub>2</sub> | CH <sub>3</sub> CHO | H <sub>2</sub> |
| FeFe <sub>2</sub> O <sub>4</sub> | 88.7 | 71.3                              | 24.3            | 2.9                 | 32.7           |
| Fe <sub>2</sub> O <sub>3</sub>   | 91.2 | 72.6                              | 23.2            | 1.1                 | 31.3           |
| Equilibrium                      | 100  | 74.21                             | 24.74           | 1.05                | 33.16          |

It can also be concluded that iron oxides have proved themselves as prospective catalysts for the production of acetone (and at the same time hydrogen) from ethanol under certain conditions.

Above 400 °C the conversion of acetone into CO<sub>2</sub> and H<sub>2</sub> becomes more significant both for FeFe<sub>2</sub>O<sub>4</sub> and for MgFe<sub>2</sub>O<sub>4</sub>, MnFe<sub>2</sub>O<sub>4</sub>, and ZnFe<sub>2</sub>O<sub>4</sub> (the selectivities toward CO<sub>2</sub> and H<sub>2</sub> increase with decrease in the selectivity to acetone) [21].

As seen from Fig. 1b, the highest and closest values for the yield of hydrogen at the ferrites MnFe<sub>2</sub>O<sub>4</sub>, MgFe<sub>2</sub>O<sub>4</sub>, and FeFe<sub>2</sub>O<sub>4</sub> were obtained at the maximum experimental temperature of 550 °C. Since magnesium is a metal with constant valence the proximity of the yields of hydrogen at MnFe<sub>2</sub>O<sub>4</sub> and MgFe<sub>2</sub>O<sub>4</sub> indicates that the Fe<sup>3+</sup> ions, which are capable of redox transitions in oxidation–reduction pairs Fe<sup>3+</sup> ↔ Fe<sup>2+</sup>, have a key role in the catalytic action of ferrites in the SRE process. The iron ions are located at least partly at the octahedral positions in the structure of the ferrites, and according to [34–36] the surface of the oxides in the spinel structure consists largely of sites of octahedral coordination, and their catalytic activity is actually determined by the octahedral cations.

The nature of the metal in the composition of the ferros spinels has a significant effect on the ability of the Fe<sup>3+</sup> cations of the spinel crystal lattice to be reduced, and this is confirmed by our data on thermoprogrammed reduction with hydrogen [21]. The lowest temperature of maximum reduction (characterizing the strength of the bond between the oxygen and the surface of the catalyst) in the investigated series of ferrites was observed for the Mn ferrite. Consequently, MnFe<sub>2</sub>O<sub>4</sub> can easily give up oxygen for oxidation of the surface organic intermediate compounds, and the selectivity to the most oxidized reaction product CO<sub>2</sub> and to hydrogen is higher for MnFe<sub>2</sub>O<sub>4</sub> than for the other ferrites.

As known, the distribution of the products of steam reforming of ethanol also depends on the acid–base characteristics of the catalysts [37–39]. According to [40–42], in the presence of a sufficient amount of weak surface acid centers the selectivity toward the aldehydes is closely related to the strength of the basic centers on the surface of the oxides; the surface weak acid centers play a key role in dehydrogenation of the alcohols. The scheme of the probable mechanism for the ferrites presented above in Fig. 3 agrees with the conclusions in the literature about the important role of both base and acid centers in the dehydrogenation of ethanol to acetaldehyde.

The data obtained by thermal programmed desorption of CO<sub>2</sub> (TPD-CO<sub>2</sub>) by the method in [21] indicate the presence of base centers on the surface of the ferrites (Table 2). The desorption maxima with temperature  $T_{m1}^{CO_2}$  in the region of 86–121 °C can be attributed to desorption of CO<sub>2</sub> from weak base centers. Here a contribution from desorption of physically adsorbed CO<sub>2</sub> cannot be entirely ruled out. The temperatures of the desorption maxima  $T_{m2}^{CO_2}$  in the region of 150–203 °C correspond to base centers of moderate strength.

Of the ferrites stable in catalysis that we studied at low degrees of conversion of ethanol (300 °C) FeFe<sub>2</sub>O<sub>4</sub> has the lowest selectivity to acetaldehyde. We note that this ferrite has the highest strength for the surface acid centers among the studied ferrites. According to the data that we obtained by thermoprogrammed desorption of ammonia (TPD-NH<sub>3</sub>) by the method in [21], the temperature of the NH<sub>3</sub> desorption maximum, which characterizes the strength of the acid centers, is

TABLE 2. Temperatures of the Desorption Maxima of Carbon Dioxide  $T_m^{\text{CO}_2}$  and Ammonia  $T_m^{\text{NH}_3}$  during TPD- $\text{CO}_2$  and TPD- $\text{NH}_3$  from the Surface of Ferrite Catalysts

| Catalyst                  | $T_{m1}^{\text{CO}_2}$ , °C | $T_{m2}^{\text{CO}_2}$ , °C | $T_m^{\text{NH}_3}$ , °C |
|---------------------------|-----------------------------|-----------------------------|--------------------------|
| $\text{FeFe}_2\text{O}_4$ | 99                          | 150                         | 372                      |
| $\text{MnFe}_2\text{O}_4$ | 115                         | 188                         | 260                      |
| $\text{MgFe}_2\text{O}_4$ | 121                         | 203                         | 205                      |
| $\text{ZnFe}_2\text{O}_4$ | 86                          | –                           | 185                      |

substantially higher for  $\text{FeFe}_2\text{O}_4$  than  $T_m^{\text{NH}_3}$  for the other ferrites (Table 2). The Zn and Mg ferrites, which have relatively weak acid centers as evidenced by low values of  $T_m^{\text{NH}_3}$  in a series of studied ferrites, have high initial selectivity to acetaldehyde.

If the temperature is increased to 400 °C the conversion of ethanol and acetaldehyde into acetone is increased, and the highest selectivity to acetone is achieved with  $\text{FeFe}_2\text{O}_4$  and  $\text{MnFe}_2\text{O}_4$  (Fig. 4). The aldol condensation includes the intermediate formation of carbanionic intermediates localized at an acid center–base center pair.

The higher selectivity to acetone in the steam reforming of ethanol on  $\text{FeFe}_2\text{O}_4$  and  $\text{MnFe}_2\text{O}_4$  can be explained by the presence on their surface of base centers of sufficient strength and acid centers that are stronger than the acid centers of the Zn and Mg ferrites, as we have demonstrated by the TPD- $\text{CO}_2$  and TPD- $\text{NH}_3$  methods.

The oxidation–reduction stages of the SRE process are characteristic primarily of the reactions in the steam conversion of ethanol (I), acetaldehyde (V), and acetone to  $\text{H}_2$  and  $\text{CO}_2$ , which take place through the formation of surface particles  $\text{CH}_{x(a)}$  and  $\text{CO}_{(a)}$ , and other intermediate compounds [23, 43]. As mentioned above, at not too high temperatures (up to 550 °C) the formation of CO in the gas phase was not observed at any of the ferrites except the Co and Ni ferrites, which were reduced to the metals during SRE. The absence of CO may be due to the fact that the adsorbed particles of CO are oxidized much more quickly to  $\text{CO}_2$  ( $\text{CO}_{(a)} + \text{O}_{(s)} \rightarrow \text{CO}_2$ ) than they are desorbed. It is also clear that Mg, Mn, Fe, Cu, and Zn ferrites are relatively inactive in water-gas shift reaction, otherwise the appearance of CO as a result of the reaction  $\text{CO}_2 + \text{H}_2 \leftrightarrow \text{CO} + \text{H}_2\text{O}$  would be observed. (According to thermodynamic calculations for the conditions used in the present work [5] the equilibrium content of CO in the products of the SRE reaction becomes appreciable above 400 °C.)

In conclusion we will briefly summarize the obtained results. The Mn, Fe, and Mg ferrites exhibit high catalytic activity in the production of hydrogen by steam reforming of ethanol. Over  $\text{MnFe}_2\text{O}_4$  a close to stoichiometric yield of hydrogen (94.6%) (5.68 mol  $\text{H}_2$ /mol of initial ethanol) is obtained at 650 °C. On Mg, Mn, Fe, Cu, and Zn ferrites it is possible to realize the reaction with complete conversion of ethanol without the formation of CO, which is an important factor for later use of the hydrogen in low-temperature fuel cells. Copper ferrite is a promising catalyst for the production of acetaldehyde from ethanol, while iron ferrite ( $\text{Fe}_3\text{O}_4$ ) is promising for acetone. These catalysts can be used in particular in two-stage catalytic processes that include the intermediate formation of acetaldehyde or acetone. The mechanism of the steam reforming of ethanol on ferrites includes both oxidation–reduction and acid–base stages. To obtain high selectivity in the process it is necessary to have a specific balance of oxidation–reduction and acid–base properties of oxide catalysts.

*The authors express their gratitude to I. V. Vasylenko for assistance in the synthesis of the catalysts and for investigating the samples by XRD, electron diffraction, and TEM. The work was conducted with financial support from a comprehensive target program of scientific investigations of the National Academy of Sciences of Ukraine “Fundamental aspects of renewable hydrogen energy and fuel cell technologies.”*

## REFERENCES

1. J. Sun and Y. Wang, *ACS Catal.*, **4**, 1078-1090 (2014).
2. A. Haryanto, S. Fernando, N. Murali, and S. Adhikari, *Energy Fuels*, **19**, 2098-2106 (2005).
3. P. D. Vaidya and A. E. Rodrigues, *Chem. Eng. J.*, **117**, 39-49 (2006).
4. M. Ni, D. Y. C. Leung, and M. K. H. Leung, *Int. J. Hydrogen Energy*, **32**, 3238-3247 (2007).
5. Y. I. Pyatnitsky, L. Yu. Dolgykh, I. L. Stolyarchuk, and P. E. Strizhak, *Teor. Éksp. Khim.*, **49**, No. 5, 265-283 (2013). [*Theor. Exp. Chem.*, **49**, No. 5, 277-297 (2013) (English translation).]
6. J. Llorca, P. R. Piscina, J. Sales, et al., *Chem. Commun.*, 641-642 (2001).
7. M. N. Barroso, M. F. Gomez, L. A. Arrua, et al., *Catal. Lett.*, **109**, 13-19 (2006).
8. H. Muroyama, R. Nakase, T. Matsui, et al., *Int. J. Hydrogen Energy*, **35**, 1575-1581 (2010).
9. Z. Li, W. Yi, and H. Qun, *Trans. Nonferrous Met. Soc. China*, **19**, 1444-1449 (2009).
10. S. Q. Chen and Y. Liu, *Int. J. Hydrogen Energy*, **34**, 4735-4746 (2009).
11. R. Espinal, E. Taboada, E. Molins, et al., *Appl. Catal. B*, **127**, 59-67 (2012).
12. V. A. de la Pena O'Shea, R. Nafria, P. Ramirez de la Piscina, et al., *Int. J. Hydrogen Energy*, **33**, 3601-3606 (2008).
13. I. L. Stolyarchuk, L. Yu. Dolgikh, I. V. Vasilenko, et al. *Teor. Éksp. Khim.*, **48**, No. 2, 119-125 (2012). [*Theor. Exp. Chem.*, **48**, No. 2, 129-134 (2012) (English translation).]
14. Y. I. Pyatnitsky, L. Yu. Dolgykh, I. L. Stolyarchuk, and P. E. Strizhak, *Teor. Éksp. Khim.*, **49**, No. 2, 99-103 (2013). [*Theor. Exp. Chem.*, **49**, No. 2, 109-114 (2013) (English translation).]
15. L. Yu. Dolgykh, I. L. Stolyarchuk, I. V. Vasilenko, et al. *Teor. Éksp. Khim.*, **49**, No. 3, 172-177 (2013). [*Theor. Exp. Chem.*, **49**, No. 3, 185-192 (2013) (English translation).]
16. L. Yu. Dolgykh, I. L. Stolyarchuk, and L. A. Staraya, *Teor. Éksp. Khim.*, **50**, No. 4, 244-247 (2014). [*Theor. Exp. Chem.*, **50**, No. 4, 245-249 (2014) (English translation).]
17. I. L. Stolyarchuk, L. Yu. Dolgikh, I. V. Vasilenko, et al., *Alternative Sources of Feedstock and Fuel. Collection of Scientific Proceedings of Academy of Sciences of Belarus, Institute of Chemistry of New Materials*, V. E. Agabekov, K. N. Gusak, Zh. V. Ignatovich (eds.) [in Russian], Belaruskaya Navuka (2014), No. 1, pp. 186-196.
18. L. Yu. Dolgykh, I. L. Stolyarchuk, L. A. Staraya, et al., *Teor. Éksp. Khim.*, **51**, No. 4, 225-229 (2015). [*Theor. Exp. Chem.*, **51**, No. 4, 230-235 (2015) (English translation).]
19. L. Yu. Dolgykh, I. L. Stolyarchuk, L. A. Staraya, et al., *Adsorp. Sci. Technol.*, **33**, Nos. 6-8, 715-721 (2015).
20. I. L. Stolyarchuk, L. Yu. Dolgykh, I. V. Vasilenko, et al., *Teor. Éksp. Khim.*, **52**, No. 4, 244-248 (2016). [*Theor. Exp. Chem.*, **52**, No. 4, 246-251 (2016) (English translation).]
21. L. Yu. Dolgikh, Y. I. Pyatnitsky, and P. E. Strizhak, *Bioethanol and Beyond: Advances in Production Process and Future Directions*, M. Brienzo (ed.), Nova Sci., New York (2018), Ch. 14, pp. 381-427.
22. I. V. Vasilenko, K. S. Gavrilenko, I. E. Kotenko, et al., *Teor. Éksp. Khim.*, **43**, No. 5, 323-329 (2007). [*Theor. Exp. Chem.*, **43**, No. 5, 353-358 (2007) (English translation).]
23. L. V. Mattos, G. Jacobs, B. H. Davis, and F. B. Noronha, *Chem. Rev.*, **112**, 4094-4123 (2012).
24. P. Ramirez de la Piscina and N. Homs, *Chem. Soc. Rev.*, **37**, 2459-2467 (2008).
25. C. Trevisanut, M. Mari, J. M. M. Millet, and F. Cavani, *J. Hydrogen Energy*, **40**, 5264-5271 (2015).
26. C. Trevisanut, F. Bosselet, F. Cavani, and J. M. M. Millet, *Catal. Sci. Technol.*, **5**, 1280-1289 (2015).
27. N. M. Schweitzer, B. Hu, U. Das, et al., *ACS Catal.*, **4**, 1091-1092 (2014).
28. B. Hu, A. Getsoian, N. M. Schweitzer, et al., *J. Catal.*, **322**, 24-37 (2015).
29. B. Hu, N. M. Schweitzer, G. Zhang, et al., *ACS Catal.*, **5**, 3494-3503 (2015).
30. D. J. Elliott and F. Pennella, *J. Catal.*, **119**, 359-367 (1989).
31. T. Nishiguchi, T. Matsumoto, H. Kanai, et al., *Appl. Catal. A*, **279**, 273-277 (2005).
32. K. Inui, T. Kurabayashi, and S. Sato, *J. Catal.*, **212**, 207 (2002).
33. I. Charkendorff and W. Niemantsverdriet, *Concepts of Modern Catalysis and Kinetics*, Wiley-VCH, Weinheim (2003).
34. J. P. Jacobs, A. Maltha, J. G. H. Reijts, et al., *J. Catal.*, **47**, 294-300 (1994).
35. C. G. Ramankutty and S. Sugunan, *Appl. Catal. A*, **218**, 39-51 (2001).

36. C. G. Ramankutty, S. Sugunan, B. Thomas, et al., *J. Mol. Catal. A*, **187**, 105-117 (2002).
37. H. Song, L. Zhang, and U. S. Ozkan, *Top. Catal.*, **55**, 1324-1331 (2012).
38. G. Garbarino, C. Wang, I. Valsamakis, et al., *Appl. Catal. B*, **174/175**, 21-34 (2015).
39. G. Busca, *Chem. Rev.*, **110**, 2217-2249 (2010).
40. C. L. Kibby and W. K. Hall, *J. Catal.*, **29**, 144-159 (1973).
41. K. Tanabe, M. Misono, Y. Ono, and H. Hattori, *New Solid Acids and Bases*, Kodansha-Elsevier, Tokyo (1989).
42. P. Canesson and M. Blanchard, *J. Catal.*, **42**, 205-212 (1979).
43. J. E. Sutton, W. Guo, M. A. Katsoulakis, et al., *Nature Chem.*, **8**, 331-337 (2016).